The molecular origins of selectivity in methanol decomposition on Pd nanoparticles

S. Schauermann, J. Hoffmann, V. Johánek, J. Hartmann, J. Libuda *, and H.-J. Freund

Fritz-Haber-Institut der Max-Planck-Gesellschaft, Faradayweg 4-6, 14195 Berlin, Germany

Received 13 August 2002; accepted 29 August 2002

We have combined multi-molecular beam methods and *in-situ* time-resolved IR reflection absorption spectroscopy (IRAS) to explore the kinetics of methanol decomposition on a supported Pd model catalyst. The well-shaped Pd nanoparticles are prepared under ultra-high vacuum conditions on a well-ordered alumina film and have previously been characterized with respect to size, density, and morphology.

Two competing decomposition pathways are observed: Whereas dehydrogenation to CO represents the dominating reaction channel, C–O bond scission proceeds at much lower rates and leads to the formation of carbon and hydrocarbon species. Using CO as a probe molecule, we show *via* IRAS spectroscopy that these carbon and hydrocarbon species preferentially block defect sites on the Pd particles such as steps or edges, whereas the (111) facet sites are affected to a lesser extent.

Employing quantitative IR\Sigma AS and steady-state isotope exchange experiments, the reaction rates for both channels are measured as a function of carbon coverage. It is found that with increasing carbon coverage, the rate of carbon formation drops rapidly, whereas the kinetics of dehydrogenation is hardly affected. These results demonstrate that the rate of C–O bond scission is drastically enhanced at the particle steps and edges, whereas for the dehydrogenation pathway this is not the case.

KEY WORDS: palladium; alumina; methanol; model catalysts; molecular beams; IR reflection absorption spectroscopy.

1. Introduction

For many reaction systems it is well known that the selectivity of supported metal catalysts may sensitively depend on the particle structure and size. In most cases, it is anticipated that such size and structure effects are related to the modified reaction properties of small aggregates in close contact with the support or the presence of specific reactive sites on the particles such as certain facets, steps, edges, and corners or interfaces (see, *e.g.*, [1,2] and references therein). Specific cases are scarce, however, in which the origins of size and structure dependencies could be uncovered on an atomic level. This lack of knowledge is a consequence of experimental difficulties arising in studies on real catalysts and the vast complexity of their surfaces.

In this work we show, for a simple model reaction system, how particle structure and selectivity are related on a microscopic level. We consider the decomposition of methanol on well-shaped Pd crystallites, which proceeds *via* two competing pathways, C–O bond scission and dehydrogenation. It is demonstrated that C–O bond scission preferentially takes place at edges and steps of the nanoparticles, whereas dehydrogenation does not.

Two experimental factors are combined to obtain this type of detailed kinetic information: First, *supported model catalysts* are employed, which facilitate a detailed structural and spectroscopic characterization and, second, a *molecular beam approach* to the kinetics is chosen, which provides detailed and quantitative data.

In the past decade a broad range of supported model catalysts has been developed, based on either oxide single crystals [3–5] or thin oxide films [6,7]. The main advantages of these models are the compatibility with most experimental methods in surface science and a reduced and controllable level of complexity [2,6]. In the specific model system used in this work, a well-ordered Al_2O_3 film on an NiAl(110) single crystal is employed as a model support [8,9]. On this support Pd particles are grown under well-controlled conditions in ultra-high vacuum (UHV). Both the geometric and electronic structure as well as the adsorption properties of these particles have been characterized previously [6,10–15].

In order to correlate structure and adsorption properties of the model systems on the one hand and their reactivity on the other, we use a molecular beam approach, combined with *in-situ* vibrational spectroscopy. Unique and detailed kinetic information can be derived from this type of experiment, as has been demonstrated for the case of CO oxidation (see [16] and references therein).

Recently, we have extended the approach to methanol decomposition as a first example of a more complex reaction system [17,18]. Reactions of methanol on Pd have attracted considerable attention due to the activity of Pd catalysts with respect to important processes such

* To whom correspondence should be addressed.
E-mail: libuda@fhi-berlin.mpg.de

1011-372X/02/1200-0209/0 © 2002 Plenum Publishing Corporation

as the synthesis as well as the partial and total oxidation of alcohols. Motivated by potential applications, a substantial amount of surface science work has been conducted on the mechanism of decomposition and oxidation of methanol on transition metal surfaces, some of which has recently been reviewed by Mavrikakis and Barteau [19]. In general, it is found that the dominant reaction pathway involves dehydrogenation to CO as the final product, *via* a methoxy species as a first intermediate [20–25]. Some controversy remains, however, with respect to the role of C–O bond scission as a pathway competing with dehydrogenation. C–O bond activation on a Pd single-crystal surface was first reported by Levis *et al.* [26,27] and later observed by several other groups as well [17,20,22,23,28]. The process leads to the formation of carbon and hydrocarbon species. In all studies, the reaction probability for C–O bond scission was observed to be low, and it has been speculated that the process might be related to the presence of specific defect sites [19,23,29].

Here, we present a detailed study on the kinetics of C–O bond scission and dehydrogenation on supported Pd particles, the first results of which have recently been published elsewhere [30]. Various types of molecular beam experiments are utilized, including two-beam isotope exchange experiments and *in-situ* time-resolved IR reflection absorption spectroscopy (TR-IRAS). It is shown how the microscopic structure of the supported Pd particles controls the selectivity toward the two decomposition pathways.

2. Experimental

All molecular beam and IRAS experiments were performed in a UHV apparatus at the Fritz-Haber-Institut (Berlin), which has been described in the literature recently [31]. The system offers the experimental possibility of up to three beams being crossed on the sample surface. The CH_3OH beams (Merck, >99.8%) were generated by effusive sources based on multi-channel arrays. For all experiments presented, the beam intensity was $5.3 \times 10^{14}\,cm^{-2}\,s^{-1}$ (or $1.5\,L\,s^{-1}$, $1\,L = 10^{-6}\,torr\,s^{-1}$ corresponds to 3.6×10^{14} CH_3OH molecules cm^{-2}). For the isotope exchange experiments a $^{12}CH_3OH$ and a $^{13}CH_3OH$ beam (Cambridge Isotope Laboratories, >99%) of equal intensity ($5.3 \times 10^{14}\,cm^{-2}\,s^{-1}$) were used. Both sources were operated at room temperature. Beam modulation was provided by a computer-controlled shutter located inside the second of two pumping stages of each beam source. To avoid artifacts due to non-homogeneous coverage, the beam diameter was chosen such that it exceeds the sample surface. For the CO sticking coefficient measurements, which were performed at a sample temperature of 300 K using a quadrupole mass spectrometer (ABB Extrel) not in line-of-sight of the sample, a CO beam was generated in a third triply differentially pumped source from a supersonic expansion. By means of a mechanical chopper the beam intensity was attenuated to $2.2 \times 10^{13}\,cm^{-2}\,s^{-1}$ and its diameter was chosen smaller than the sample. Corresponding IR spectra as a function of coverage were measured under identical conditions with a beam size exceeding the sample surface. All IR spectra were acquired employing a vacuum FT-IR spectrometer (Bruker IFS 66v) at a spectral resolution of $2\,cm^{-1}$, using a MIR polarizer to select the p-component of the IR light only. For the time-resolved spectra, several isotope exchange cycles were accumulated to improve the signal/noise ratio. Typically, the total acquisition time per spectrum was 10 s for the time-resolved spectra and 140 s otherwise.

The X-ray photoelectron spectra (XPS) were recorded in a second UHV system using a non-monochomatized Mg K_α source and a hemispherical analyzer (Specs). High background pressures during gas exposure were avoided by using a doser system.

The alumina film was prepared by sputtering and annealing of an NiAl(110) single crystal, followed by an oxidation and annealing procedure, the details of which are given elsewhere [9,32]. Cleanliness and quality of the oxide film were checked *via* low energy electron diffraction (LEED) and Auger electron spectroscopy (AES). Before the experiment, the Pd (>99.9%) was deposited using a commercial evaporator (Focus, EFM 3) based on electron bombardment (Pd coverage: $2.7 \times 10^{15}\,cm^{-2}$, sample temperature: 300 K). During deposition, the crystal was biased with a retarding voltage in order to prevent ions from being accelerated towards the sample (point-defect creation). The evaporator flux was calibrated by a quartz microbalance prior to use. After preparation, the Pd particles were stabilized by oxygen and CO exposure as discussed previously [13,15].

3. Results and discussion

Before exploring the kinetics of methanol decomposition, it is essential briefly to reconsider the structure of the Pd particles on Al_2O_3/NiAl(110) used in this study. In figure 1 a scanning tunneling microscopy (STM) image of the model system is displayed. The particles are characterized by an average size of approximately 5.5 nm and contain about 3000 Pd atoms each. The majority of particles exhibit the morphology of well-shaped crystallites. These crystallites grow in (111) orientation and are predominantly terminated by (111) facets. Additionally, a small fraction of (100) facets are exposed. For the current study the presence of edge and step sites is of particular relevance. About one-third of the top facet atoms are located at the facet edge for the given particle size. Additionally, steps can be found on some top facets and contribute to the fraction of defect sites (compare to model in [33]). Further structural details are given elsewhere [13].

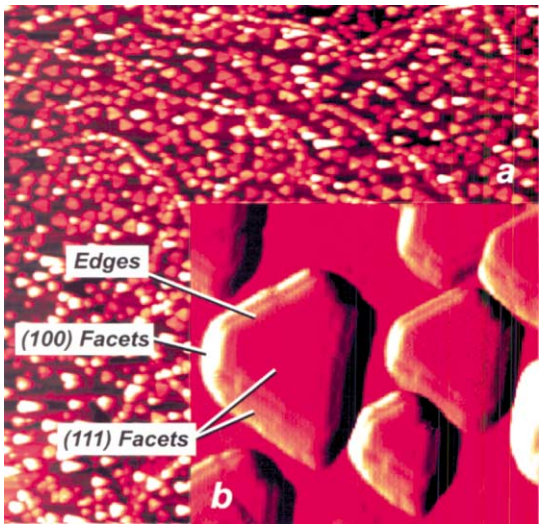

Figure 1. (a) STM image (CCT, Constant Current Topography, 3000 Å × 3000 Å) of the Pd particles grown at 300 K on Al_2O_3/NiAl(110); (b) differentiated close-up STM image of the Pd particles (200 Å × 200 Å), from [13].

Recently, we have studied the mechanism [17] and the kinetics [18] of methanol decomposition and oxidation on Pd/Al_2O_3/NiAl(110). In accordance with the single-crystal results discussed before (see introduction), adsorbed molecular CH_3OH was found to dissociate partially to form methoxy species. This intermediate rapidly undergoes dehydrogenation to CO at temperatures above 200 K. CO itself desorbs over a broad temperature range with a main desorption feature around 480 K in a temperature-programmed desorption (TPD) experiment (slightly depending on particle size [15]).

In addition to dehydrogenation, which represents the dominating reaction channel, there is experimental evidence for CO bond scission from XPS, IRAS, and TPD experiments, as summarized in figure 2. In a photoelectron spectrum of the C 1s region recorded directly after preparation, no atomic carbon is found on the pristine model catalyst (see figure 2(a), spectrum 1). Adsorbed CO, however, is identified *via* the feature at 286 eV binding energy (BE) and the satellite structure around 292 eV BE (compare [34,35]). After extended exposure to methanol a second intense feature around 284 eV BE appears (see figure 2(a), spectrum 2). Based on a comparison with single-crystal data, this low BE peak can be assigned to the formation of carbon atoms and hydrocarbon moieties (see [20] and references therein). It is noteworthy that these carbon species can be easily removed by exposure to moderate amounts of oxygen at elevated temperature (see figure 2(a), spectrum 3).

Additional evidence for carbon accumulation is provided by IRAS spectra, acquired *in situ* during exposure of a continuous CH_3OH beam at a surface temperature of 440 K (see figure 2(b)). As expected, dehydrogenation leads to a rapid build-up of a steady-state CO coverage, as identified by the characteristic IR absorption in the CO-stretching frequency region. Briefly, the main peak around 1900 cm^{-1} and the shoulder at 1830 cm^{-1} are assigned to CO adsorbed on different types of hollow sites on (111) facets, with some contributions from defects and (100) facets. A detailed discussion of the CO spectra can be found elsewhere (see, *e.g.*, [12,16,36] and references therein). Here, the most important point is that with increasing exposure time a slowly decreasing CO absorption signal is observed. In accordance with the XPS results, the loss in CO adsorption capacity is attributed to a slow poisoning of the particles by carbon and hydrocarbon species. Direct evidence for the presence of hydrocarbon species is derived from the spectra of the CH-stretching frequency region, where weak features at 2945 and 2830 cm^{-1} are observed. Previously, absorption bands at 2887, 2976 [37] and 2920 cm^{-1} [38] have been observed for CH_3 on Pd. It should also be noted that hydrocarbon species formed *via* methanol decomposition on Pd have been shown to be stable at temperatures of 500 K [23].

In addition to the IR data, TPD spectra support the assumption that both carbon and hydrocarbon species are accumulated on the model catalyst. Desorption peaks at 15 amu between 600 and 800 K and at 28 amu around 800 K are observed after extended methanol exposure (see figure 2(c)). Whereas the first feature indicates desorption of hydrocarbons, the second feature is related to recombinative desorption of CO produced from coadsorbed carbon and oxygen [39] (note that a background signal at 15 and 28 amu arises from fragmentation of methanol desorbing from the sample holder and manipulator, see trace at 31 amu in figure 2(c)).

It is essential to note that upon CO exposure no similar poisoning effect is observed on the same Pd particle system [40]. From this we can infer that the carbon deposits do not originate from CO decomposition, but from scission of the C−O bond during the dehydrogenation process itself.

The question arises whether specific sites on the particles can be identified at which the carbon deposits accumulate. Here we can take advantage of the large amount of vibrational data which is available on CO adsorption on Pd single crystals and supported Pd particles and use CO as a sensitive probe molecule. For this purpose a well-defined CO coverage is prepared on the model catalyst by exposing the surface to CO at 300 K (20 L CO). Subsequently, the sample is cooled to 100 K to improve the spectral resolution and an IR spectrum is recorded. The procedure is performed both for the pristine Pd particles immediately after preparation and for the partially-carbon-covered sample after extended exposure to methanol at 440 K (~7000 L, 2.5×10^{18} molecules cm^{-2}).

The corresponding spectra for the clean and C-covered surface and a difference spectrum are displayed in figure 3. For the pristine sample, the spectrum is

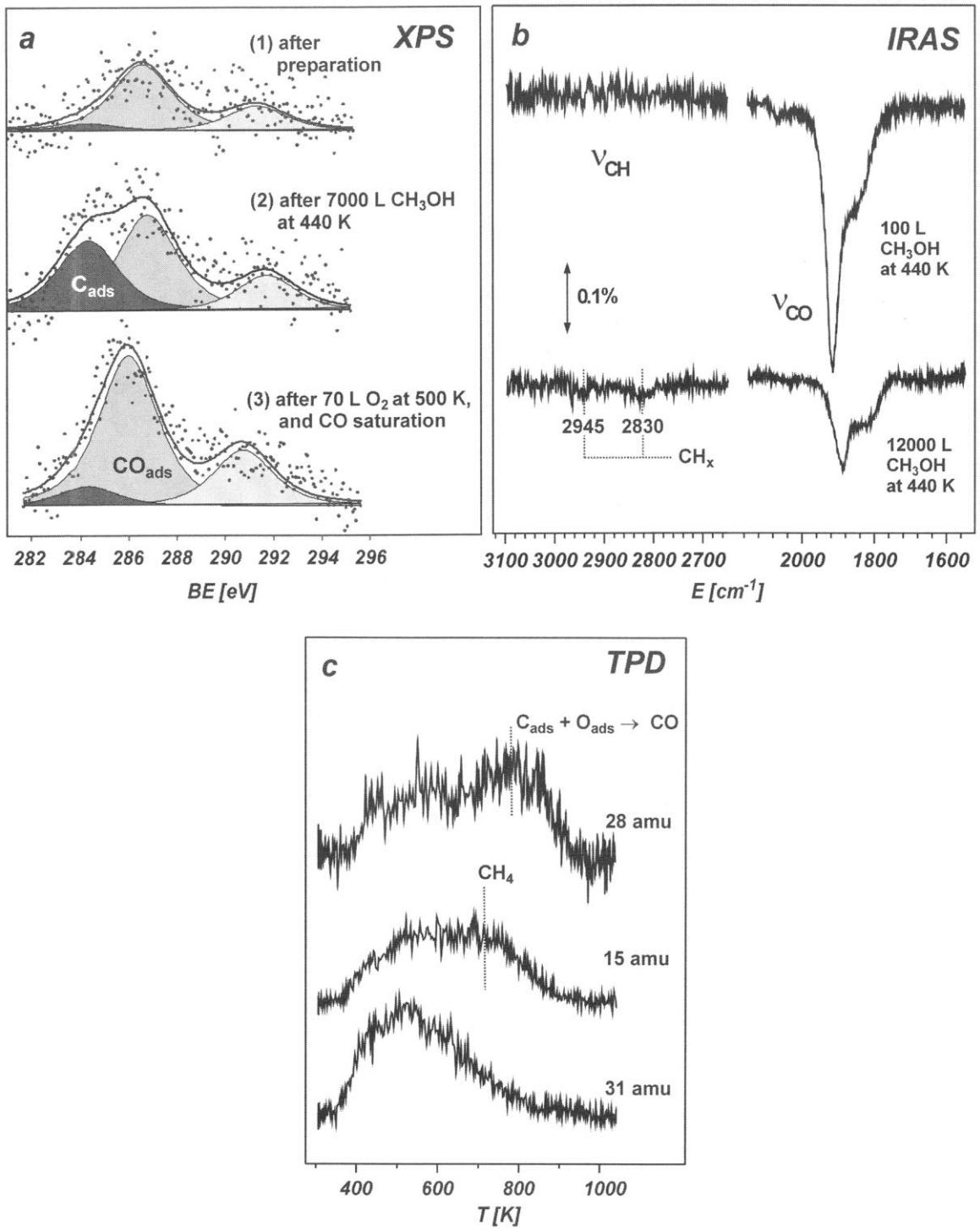

Figure 2. (a) XPS spectra of the C 1s region recorded at 300 K (1) after preparation of the PdPd/Al_2O_3/NiAl(110) model catalyst, (2) after extended exposure to methanol at 440 K and (3) after oxygen dosage at 500 K followed by CO saturation at 300 K; (b) IR reflection absorption spectra recorded during methanol exposure at 440 K immediately after preparation and after extended exposure to methanol; (c) TPD spectra recorded after extended exposure to methanol at 440 K.

dominated by a sharp absorption feature at around 1960 cm^{-1}. A broad low-frequency shoulder starts at approximately 1930 cm^{-1} and extends to approximately 1840 cm^{-1}. Additionally, a weak feature at 2075 cm^{-1} is observed. Previously, these absorption bands have been discussed in detail and assigned in the following manner [12,16,36]: The features between 1930 and 1840 cm^{-1} are assigned to CO adsorbed mainly on hollow sites on Pd(111), whereas the absorption peak at 2075 cm^{-1} is related to on-top CO, presumably on Pd(111) facets and on defects. The most interesting feature is the intense band at 1960 cm^{-1}. A detailed

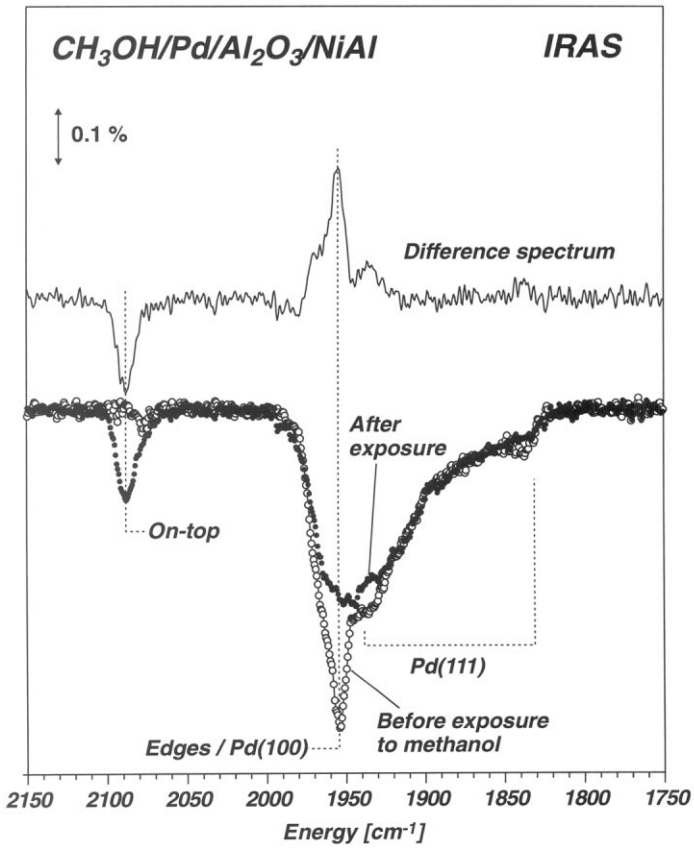

Figure 3. IR reflection absorption spectra of the CO stretching frequency region for $Pd/Al_2O_3/NiAl(110)$, taken at a sample temperature of 100 K after CO exposure at 300 K (~20 L). Open symbols: immediately after preparation; solid symbols: after extended exposure to methanol at 440 K (7000 L). Solid line: difference spectrum for the two situations.

comparison with previous work [12,36] shows that this absorption corresponds to a feature which as a function of coverage appears in the range between approximately 1950 and 2000 cm^{-1}. It was suggested that this signal originates from a superposition of bridge-bonded CO on (100) facets and defect sites such as particle edges or steps [12,36]. Taking into account the morphology and epitaxial orientation of the Pd particles, the contribution of (100) facets, however, is expected to be minor (as a consequence of the metal surface selection rule, which is also valid for sufficiently thin metal-supported oxide films, the IR absorption is attenuated on facets, which, like the (100) facets, are tilted with respect to the surface normal; see, *e.g.*, [41]). Following these arguments, we assume that the absorption feature at 1960 cm^{-1} is dominated by CO adsorbed at defect sites, mainly at particle edges and steps (compare figure 1). This assignment has recently been corroborated by a density functional theory (DFT) study investigating CO adsorption at different sites of Pd nanoparticles [42]. In this work, CO was found to adsorb strongly at bridge sites on particle edges and the corresponding species was assigned to the absorption feature under discussion.

If an equivalent IR experiment is performed after extended exposure to methanol at 440 K, drastic changes are observed in the spectra (see figure 3). The defect peak at 1960 cm^{-1} vanishes almost completely, whereas the absorption signal in the on-top region strongly increases (2085 cm^{-1}). All other features in the spectrum, in particular the region below 1950 cm^{-1} (regular facets), remain nearly unaffected (see difference spectrum in figure 3).

From this observation it is concluded that the carbon species have a pronounced influence on adsorption at the particle steps and edges only. Here, however, the CO adsorption behavior is strongly modified, including a reduced adsorption energy—most probably a change in the adsorption site. A more detailed characterization of the carbon species itself is not possible on the basis of the present data. It is noteworthy, however, that carbon adsorption on Pd clusters was recently investigated theoretically and similar adsorption energies for surface and subsurface species were found [42]. An influence of these carbon species on the CO adsorption behavior was predicted, which is compatible with the effects observed experimentally.

It should be kept in mind, however, that the IR signals originating from the regular facets and from the defects are expected to be strongly modified by dipole coupling effects [43]. As a consequence, the relative intensities do not directly reflect the relative amount of CO adsorbed at the corresponding sites (see

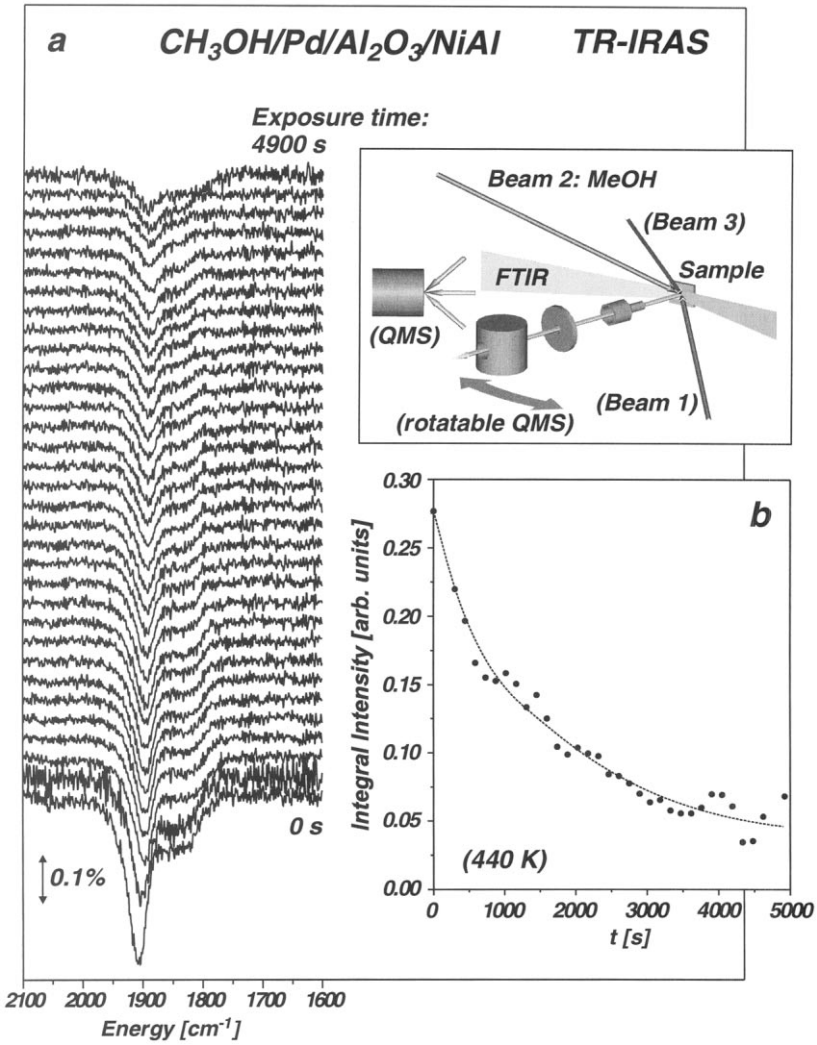

Figure 4. (a) IR reflection absorption spectra of the CO stretching frequency region for $Pd/Al_2O_3/NiAl(110)$ as a function of exposure time to the methanol beam (beam intensity: 5.3×10^{14} molecules $cm^{-2}\,s^{-1}$; surface temperature of 440 K); (b) integral absorption in the CO stretching frequency region as a function of exposure time.

[36] and references therein). Instead, the defect feature at high frequency is expected to gain intensity at the expense of the absorption signal originating from the facets. Although the coupling effects preclude an exact quantification, it is apparent from these observations that adsorption at particle defect sites (*i.e.*, steps and edges) is blocked or strongly modified by carbon species, which preferentially accumulate at these sites during methanol decomposition.

In the second part of this study, we explore how the kinetics of the two reaction pathways is affected by the carbon accumulation process. First we focus on the rate of C–O bond breakage. In order to quantify the fraction of the surface poisoned by carbon, we proceed as follows: First, time-resolved IR spectra are recorded during methanol decomposition. The corresponding spectra are displayed in figure 4(a). As discussed before, we observe a slowly decreasing absorption in the CO stretching frequency region. Quantitatively, this effect is shown in figure 4(b), where the integral absorption in the CO region is displayed as a function of exposure time.

In order to convert the integral absorption into coverage, a calibration procedure is applied. For this purpose, the integral CO absorption is estimated as a function of coverage by combining a CO sticking coefficient measurement and TR-IR spectroscopy. As the result of this type of experiment, the IR absorption is obtained as a function of surface coverage. A corresponding plot for the $CO/Pd/Al_2O_3$ model catalyst is displayed in figure 5(b). As previously observed for other systems (see *e.g.*, [41] and references therein), the integral absorption increases rapidly with coverage in the low coverage regime, whereas at high coverage the dependence becomes much weaker. The calibration is used to estimate the amount of CO present on the partially carbon-covered samples $\theta_{CO}(t)$ and the surface fraction covered by carbon $(\theta_{CO}(0) - \theta_{CO}(t)$, where

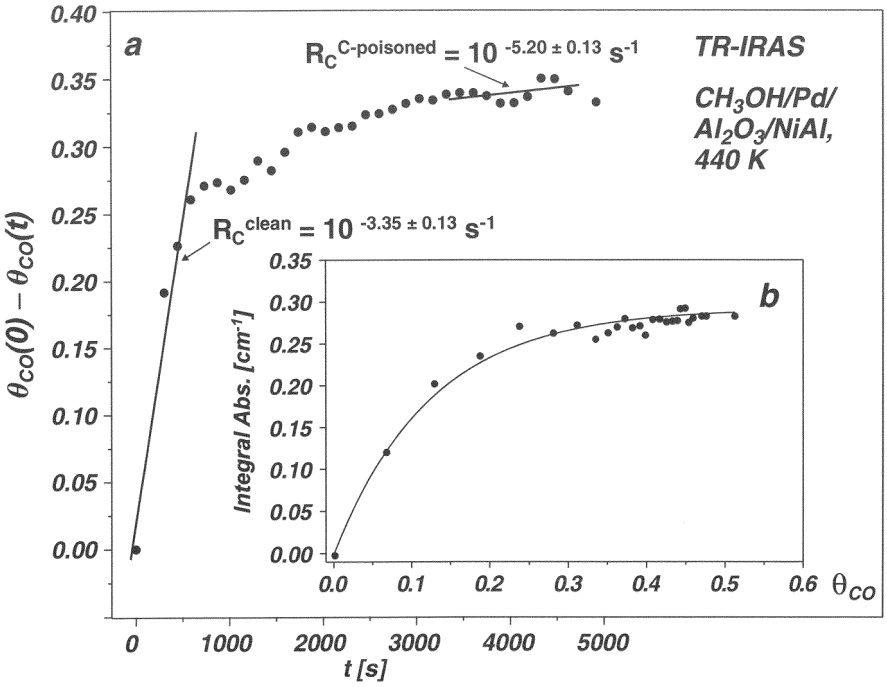

Figure 5. (a) Change in the CO coverage as a function of exposure time to the methanol beam (intensity: 5.3×10^{14} molecules cm^{-2} s^{-1}; surface temperature of 440 K) as derived from the IR spectra displayed in figure 2; (b) integral CO absorption signal as a function of CO coverage, extracted from a combined sticking-coefficient/TR-IRAS experiment.

$\theta_{CO}(0)$ is the initial CO coverage). The result is shown in figure 5(a) as a function of exposure time to the methanol beam. It is apparent that initially the rate of carbon formation is high, but the process decelerates rapidly with increasing carbon coverage. Additionally, a rough estimate of the rate of carbon formation $R_C = d(\theta_{CO}(0) - \theta_{CO}(t))/dt$ can be derived from these data (see figure 5(a)). On the pristine model catalyst a rate of $R_C^{clean} = 10^{-3.35 \pm 0.13}\ s^{-1}$ is calculated, whereas on the partially-C-covered catalyst the rate drops to a value of $R_C^{C\text{-poisoned}} = 10^{-5.20 \pm 0.13}\ s^{-1}$ (after exposure to the methanol beam for 4000 s at 440 K, $\sim 2 \times 10^{18}$ molecules cm^{-2}, 6000 L). This observation indicates that C–O bond breakage is fast only at the defect sites, which are preferentially poisoned with increasing carbon coverage, but not at the regular facet sites.

The last question to ask is whether the second reaction pathway, *i.e.*, the methanol dehydrogenation, is affected by carbon accumulation in a similar manner. Here, we are facing the experimental problem that the fragmentation pattern of CH_3OH containing $m/e = 28$ as a main fragment and the low reaction probabilities prevent direct rate measurements *via* the gas phase. As demonstrated previously, the problem can be circumvented by performing isotope exchange experiments combined with TR-IRAS [18]. The setup is schematically displayed in figure 6(a). We expose the sample to a constant flux of methanol, switching between a $^{12}CH_3OH$ beam and a $^{13}CH_3OH$ beam of equal intensity. Formation of CO *via* methanol dehydrogenation and CO desorption result in an exchange of ^{12}CO and ^{13}CO on the surface, and the corresponding time constant for CO exchange τ_{CO} can be determined by TR-IRAS. A typical exchange experiment is displayed in figure 6(b). The stretching vibrations of ^{12}CO and ^{13}CO with maxima at 1900 and 1860 cm^{-1}, respectively, can be distinguished clearly. In order to extract the exchange kinetics from these data, we calculate an average absorption frequency for each spectrum (figure 5(c)). From the time dependence of the average absorption frequency, which shows an exponential behavior, τ_{CO} is determined. In this manner, we obtain $1/\tau_{CO}^{clean} = 10^{-1.01 \pm 0.13}\ s^{-1}$ for the pristine sample and $1/\tau_{CO}^{C\text{-poisoned}} = 10^{-0.85 \pm 0.17}\ s^{-1}$ on the partially C-covered surface (methanol exposure $\sim 2.5 \times 10^{18}$ molecules cm^{-2}, 7000 L, surface temperature 440 K). As a second point, the CO steady-state coverage can be estimated as $\theta_{CO}^{clean} = 0.15 \pm 0.07$ and $\theta_{CO}^{C\text{-poisoned}} = 0.04 \pm 0.02$ from the static CO spectra *via* the coverage–absorption relationship used before (see figure 5(b)). From both pieces of information, the CO coverages and the exchange time constants, the rates of CO formation (or methanol dehydrogenation) are derived as $R_{CO}^{clean} = \theta_{CO}^{clean}/\tau_{CO}^{clean} = 10^{-1.82 \pm 0.35}\ s^{-1}$ on the clean sample and $R_{CO}^{C\text{-poisoned}} = \theta_{CO}^{C\text{-poisoned}}/\tau_{CO}^{C\text{-poisoned}} = 10^{-2.22 \pm 0.39}\ s^{-1}$ on the carbon-poisoned sample.

The results for the two reaction pathways show that the ratio between the rate of dehydrogenation and the rate of C–O bond scission R_{CO}/R_C increases from 30 on the pristine sample to $\sim$1000 on the carbon-contaminated surface. This effect is a consequence of the rapidly-dropping rate of C–O bond scission with increasing carbon coverage. At the same time the

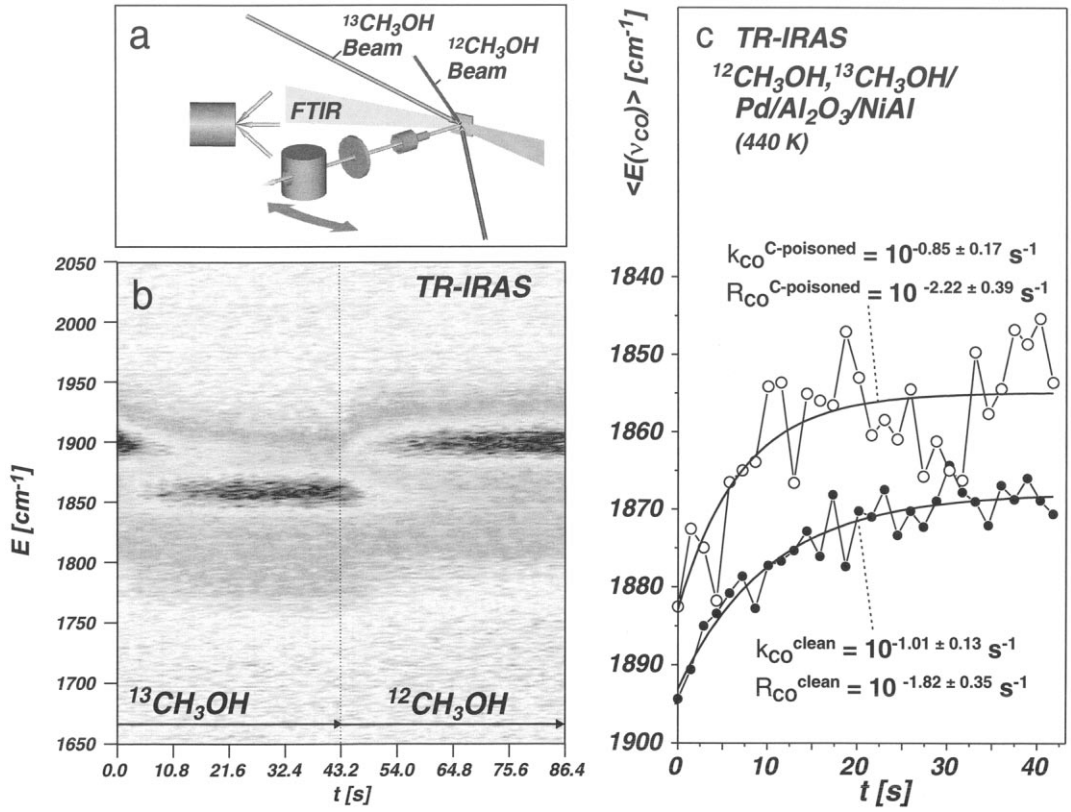

Figure 6. (a) Schematic setup of the isotopic exchange experiment for CO formation/desorption rate measurements; (b) TR-IR reflection absorption spectra for the $^{13}CH_3OH/^{12}CH_3OH$ recorded during an isotopic exchange experiment (440 K); (c) rates and time constants for CO formation/desorption on the Pd/Al_2O_3/NiAl(110) model catalyst directly after preparation (solid symbols) and after extended exposure to methanol at 440 K (7000 L) (open symbols) as determined from the average IR absorption energy in the CO stretching frequency region (see text).

decrease in the rate of dehydrogenation is moderate only and roughly reflects the decrease in the C-free Pd surface area.

4. Conclusions

In this study, we have employed molecular beam methods coupled with TR-IRAS to investigate the selectivity and kinetics of methanol decomposition on a supported Pd model catalyst. The model surface was prepared under UHV conditions on a well-ordered alumina film on an NiAl(110) single crystal and it is characterized by well-shaped Pd crystallites exposing predominantly (111) facets and a small fraction of (100) facets.

1. Two pathways of methanol decomposition are observed: rapid dehydrogenation to CO and slow C–O bond scission leading to formation of carbon and hydrocarbon species. Accumulation of these carbon and hydrocarbon species is proven by XPS, IRAS, and TPD.
2. Employing CO as a probe molecule, it is shown that the carbon and hydrocarbon species formed during C–O bond scission are not evenly distributed over the model surface but preferentially accumulate at defect sites on the Pd particles, *i.e.*, at steps and at particle edges.
3. Via TR-IRAS and isotope exchange experiments it is shown that with increasing carbon and hydrocarbon coverage, the rate of carbon accumulation drops rapidly, whereas the kinetics of dehydrogenation remains largely unaffected. From this it is concluded that C–O bond scission preferentially occurs at particle step and edge sites, whereas this is not the case for the dehydrogenation.

Acknowledgments

This project has been funded by the Max-Planck-Society and the Deutsche Forschungsgemeinschaft. The authors are grateful to M. Bäumer, M. Heemeier, and M. Naschitzki for support with respect to the acquisition and evaluation of the STM and XPS data used in this publication.

References

[1] V.P. Zhdanov and B. Kasemo, Surf. Sci. Rep. 39 (2000) 25.
[2] C.R. Henry, Surf. Sci. Rep. 31 (1998) 231.

[3] C.R. Henry, C. Chapon, C. Duriez and S. Giorgio, Surf. Sci. 253 (1991) 177.
[4] C.T. Campbell, A.W. Grant, D.E. Starr, S.C. Parker and V.A. Bondzie, Topics Catal. 14 (2001) 43.
[5] V. Nehasil, T. Hrncir, S. Zafeiratos, S. Ladas and V. Matolin, Surf. Sci. 454 (2000) 289.
[6] M. Bäumer and H.-J. Freund, Prog. Surf. Sci. 61 (1999) 127.
[7] T.P. St. Clair and D.W. Goodman, Topics Catal. 13 (2000) 5.
[8] R.M. Jaeger, H. Kuhlenbeck, H.-J. Freund, M. Wuttig, W. Hoffmann, R. Franchy and H. Ibach, Surf. Sci. 259 (1991) 235.
[9] J. Libuda, F. Winkelmann, M. Bäumer, H.-J. Freund, T. Bertrams, H. Neddermeyer and K. Müller, Surf. Sci. 318 (1994) 61.
[10] M. Bäumer, J. Libuda and H.-J. Freund, in: *Chemisorption and Reactivity on Supported Clusters and Thin Films*, ed. R.M. Lambert and G. Pacchiono (Kluwer, Dordrecht, 1997) p. 61.
[11] K.H. Hansen, T. Worren, S. Stempel, E. Laegsgaard, M. Bäumer, H.-J. Freund, F. Besenbacher and I. Stensgaard, Phys. Rev. Lett. 83 (1999) 4120.
[12] M. Frank and M. Bäumer, Phys. Chem. Chem. Phys. 2 (2000) 3723.
[13] I. Meusel, J. Hoffmann, J. Hartmann, M. Heemeier, M. Bäumer, J. Libuda and H.-J. Freund, Catal. Lett. 71 (2001) 5.
[14] S. Shaikhutdinov, M. Frank, M. Bäumer, S.D. Jackson, R. Oldman, J.C. Hemminger and H.-J. Freund, Catal. Lett. 80 (2002) 115.
[15] S. Shaikhutdinov, M. Heemeier, J. Hoffmann, I. Meusel, B. Richter, M. Bäumer, H. Kuhlenbeck, J. Libuda, H.-J. Freund, R. Oldman, S.D. Jackson, C. Konvicka, M. Schmid and P. Varga, Surf. Sci. 501 (2002) 270.
[16] J. Libuda and H.-J. Freund, J. Phys. Chem. B 106 (2002) 4901.
[17] S. Schauermann, J. Hoffmann, V. Johánek, J. Hartmann and J. Libuda, Phys. Chem. Chem. Phys. 4 (2002) 3909.
[18] J. Hoffmann, S. Schauermann, V. Johánek, J. Hartmann and J. Libuda, J. Catal. (accepted).
[19] M. Mavrikakis and M.A. Barteau, J. Mol. Catal. A 131 (1998) 135.
[20] J.-J. Chen, Z.-C. Jiang, Y. Zhou, B.R. Chakraborty and N. Winograd, Surf. Sci. 328 (1995) 248.
[21] F. Solymosi, A. Berko and Z. Toth, Surf. Sci. 285 (1993) 197.
[22] M. Rebholz, V. Matolin, R. Prins and N. Kruse, Surf. Sci. 251 (1991) 1117.
[23] M. Rebholz and N. Kruse, J. Chem. Phys. 95 (1991) 7745.
[24] A.K. Bhattacharya, M.A. Chesters, M.E. Pemble and N. Sheppard, Surf. Sci. 206 (1988) L845.
[25] K. Christmann and J.E. Demuth, J. Chem. Phys. 76 (1982) 6318.
[26] R.J. Levis, Z.C. Jiang and N. Winograd, J. Am. Chem. Soc. 111 (1989) 4605.
[27] R.J. Levis, Z.C. Jiang and N. Winograd, J. Am. Chem. Soc. 110 (1988) 4431.
[28] N. Kruse, M. Rebholz, V. Matolin, G.K. Chuah and J.H. Block, Surf. Sci. Lett. 238 (1990) L457.
[29] R.P. Holroyd and M. Bowker, Surf. Sci. 377–379 (1997) 786.
[30] S. Schauermann, J. Hoffmann, V. Johánek, J. Hartmann, J. Libuda and H.-J. Freund, Angew. Chem. Int. Ed. 41 (2002) 2513.
[31] J. Libuda, I. Meusel, J. Hartmann and H.-J. Freund, Rev. Sci. Instrum. 71 (2000) 4395.
[32] R.M. Jaeger, J. Libuda, M. Bäumer, K. Homann, H. Kulenbeck and H.-J. Freund, J. Electron Spectrosc. Relat. Phenom. 64/65 (1993) 217.
[33] J. Hoffmann, S. Schauermann, J. Hartmann, V.P. Zhdanov, B. Kasemo, J. Libuda and H.-J. Freund, Chem. Phys. Lett. 354 (2002) 403.
[34] A. Sandell, J. Libuda, P.A. Brühwiler, S. Andersson, M. Bäumer, A.J. Maxwell, N. Mårtensson and H.-J. Freund, Phys. Rev. B 55 (1997) 7233.
[35] A. Sandell, A. Beutler, R. Nyholm, J.N. Andersson, P.A. Brühwiler, N. Martensson, J. Libuda, K. Wolter, O. Seiferth, M. Bäumer, H. Kuhlenbeck and H.-J. Freund, Phys. Rev. B 57 (1998) 13199.
[36] K. Wolter, O. Seiferth, H. Kuhlenbeck, M. Bäumer and H.-J. Freund, Surf. Sci. 399 (1998) 190.
[37] K. Wolter, PhD Thesis, Berlin, 2001.
[38] J. Raskó, J. Bontovics and F. Solymosi, J. Catal. 143 (1993) 138.
[39] V. Matolin, M. Rebholz and N. Kruse, Surf. Sci. 245 (1991) 233.
[40] J. Libuda, I. Meusel, J. Hoffmann, J. Hartmann, L. Piccolo, C.R. Henry and H.-J. Freund, J. Chem. Phys. 114 (2001) 4669.
[41] F.M. Hoffmann, Surf. Sci. Rep. 3 (1983) 107.
[42] I.V. Yudanov, R. Sahnoun, K.M. Neyman and N. Rösch (in preparation).
[43] P. Hollins, Surf. Sci. Rep. 16 (1992) 51.